Vibrational Spectroscopy 63 (2012) 325–337

Contents lists available at SciVerse ScienceDirect

Vibrational Spectroscopy

journal homepage: www.elsevier.com/locate/vibspec

Conformational behaviour of antioxidant chromones. A vibrational spectroscopy study

N.F.L. Machado[a], R. Valero[a], H.S. Domingos[a], J. Tomkinson[b], L.A.E. Batista de Carvalho[a], J.C. Otero[c], M.P.M. Marques[a,d,*]

[a] Research Unit "Molecular Physical-Chemistry", University of Coimbra, Portugal
[b] ISIS Facility, STFC Rutherford Appleton Laboratory, Chilton, United Kingdom
[c] Department of Physical-Chemistry, Faculty of Science, University of Malaga, Spain
[d] Department of Life Sciences, Faculty of Science and Technology, University of Coimbra, Portugal

ARTICLE INFO

Article history:
Received 13 April 2012
Received in revised form 26 June 2012
Accepted 26 June 2012
Available online 30 August 2012

Keywords:
Phytochemicals
H-bonding profile
Raman
Infrared
Inelastic neutron scattering
Cancer chemoprevention

ABSTRACT

Chromone and two carboxylic derivatives – chromone-2-carboxylic acid (2CA) and chromone-3-carboxylic acid (3CA) – were investigated as to their conformational preferences by vibrational spectroscopy – Raman, FTIR and INS – combined to density functional theory and plane-wave calculations. INS experiments allowed to clearly detect intramolecular hydrogen-type close contacts in these systems. A natural bond orbital (NBO) analysis was performed, including calculation of the second-order perturbation energies ($E^{(2)}$) and orbital occupancies, to provide theoretical evidence of the stabilisation due to the $\pi_i^* \rightarrow \pi_j^*$ donor–acceptor interaction. A complete assignment of the vibrational spectra was achieved for all compounds, allowing us to determine their most stable conformers and establish their H-bonding profile. 3CA was shown to display a particularly strong intramolecular H-bond, which can explain its singular conformational behaviour and abnormally high pK_a value.

1. Introduction

Chromones (1-benzopyran-4-ones, Fig. 1) are naturally occurring compounds present in representative amounts in a normal human diet, displaying a wide range of biological activities (*e.g.* anti-inflammatory and anticancer) due to their well-recognised antioxidant properties [1–3]. Since oxidative damage in numerous cell targets (DNA, lipids, and proteins) is known to be directly linked to a number of severe pathologies, namely liver toxicity, cardiovascular and neurodegenerative disorders (*e.g.* Alzheimer and Parkinson's) and cancer, which are a major cause of death worldwide, the design of new antioxidant agents from natural sources has been the object of vigorous study in the last decade, with a view to establishing successful chemopreventive strategies as well as chemotherapeutic alternatives (*e.g.* combination therapy). The development of new chromone-based protective, and potentially therapeutic, agents is an important research area in Medicinal Chemistry, the chromone core being a key element of pharmacophores of many biologically active molecules displaying diverse medicinal applications.

These prospective health benefits arising from the antioxidant capacity of chromone derivatives are ruled by strict structure–activity relationships (SAR's), which, apart from determining their biological action, modulate their systemic distribution and bioavailability in sites of oxidation within the cell. Conformational preferences such as flexibility, formation of hydrogen bonds – both intra- and intermolecular – and planar or skewed relative orientations of the substituent groups linked to the chromone skeleton determine the properties of the systems. The possibility of occurrence of hydrogen close contacts, for instance, can lead to a quite large stabilisation and therefore to a marked preference for a particular conformation as opposed to other likely geometries [2]. Additionally, there is no available X-ray crystallography data for either chromone or the carboxylate derivatives presently studied. It is therefore essential to obtain an accurate conformational analysis of this kind of systems in order to clearly understand their mode of action and to establish reliable SAR's, crucial for a rational design of effective chemopreventive/therapeutic agents against cancer. Such goal can be attained through the combined use of spectroscopic techniques and theoretical approaches, in order to determine the compounds' most stable structures, as well as their main conformational preferences and possible interactions with biological targets and receptors.

* Corresponding author at: Research Unit "Molecular Physical-Chemistry", University of Coimbra, 3001-401 Coimbra, Portugal. Tel.: +351 239826541; fax: +351 239854448.
E-mail address: pmc@ci.uc.pt (M.P.M. Marques).

0924-2031/$ – see front matter © 2012 Elsevier B.V. All rights reserved.
http://dx.doi.org/10.1016/j.vibspec.2012.06.010

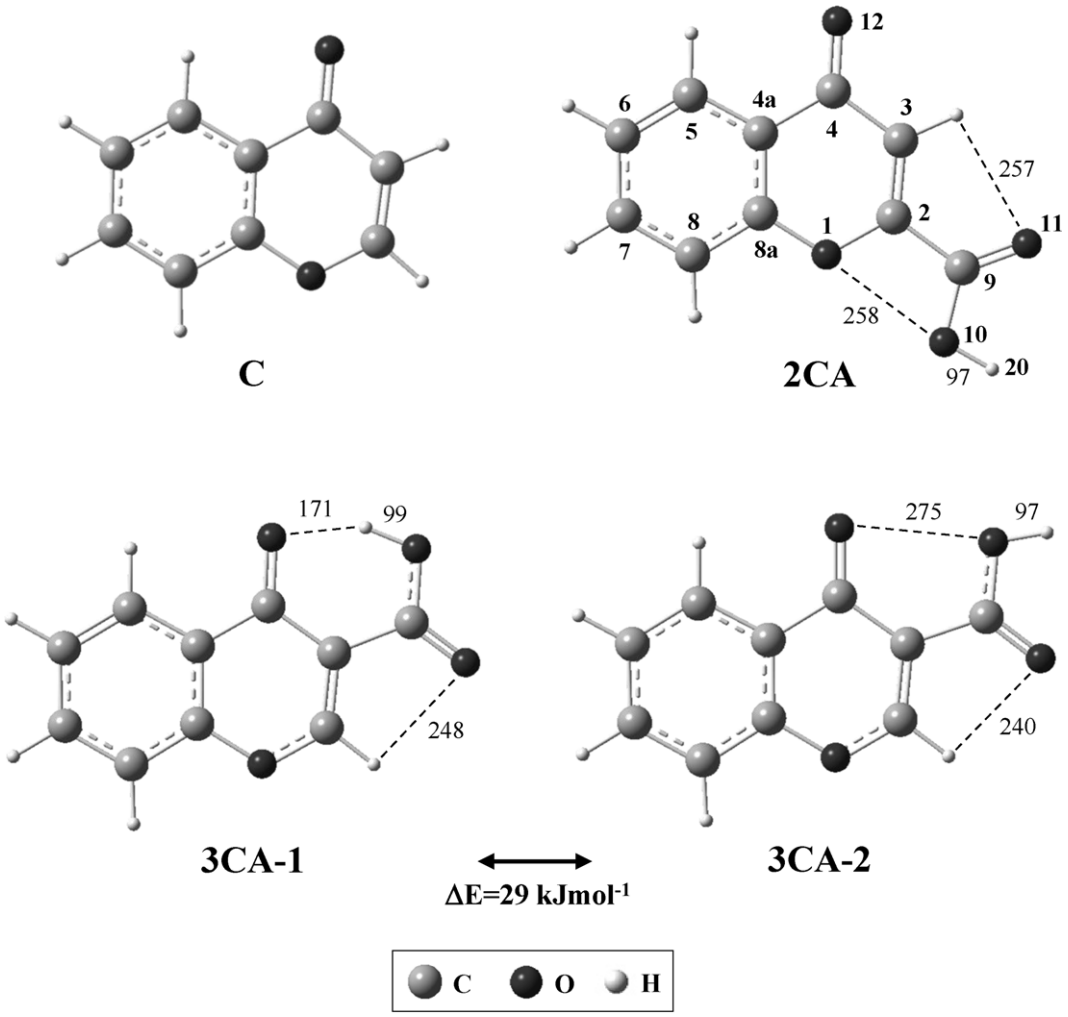

Fig. 1. Calculated (B3LYP/6-31G**) structures for chromone (C) and its carboxylic derivatives 2CA (lowest energy conformer) and 3CA (most stable conformers) (the atom numbering is included. Distances are in pm).

The use of vibrational spectroscopy – infrared, Raman and inelastic neutron scattering (INS) – is a reliable and accurate procedure for this kind of studies, since it allows analysis of samples both in the solid state and in solution, for distinct conditions (*e.g.* pH and temperature) and in a wide concentration range. INS, in particular, is a well suited technique to the study of hydrogenous compounds such as the ones presently investigated. Actually, the neutron scattering cross-section of an atom (σ) is characteristic of that atom and independent of its chemical environment. Since the value for hydrogen (80 barns) far exceeds that of all other elements (typically *ca.* 5 barns), the modes of significant hydrogen displacement (u_i) dominate the INS spectra [4]. For a mode at a given energy ν_i, the intensity from a powdered sample obeys the simplified relationship

$$S_i(Q, \nu_i) = \frac{(Q^2, u_i^2)\sigma}{3} \exp\left(-\frac{Q^2\alpha_i^2}{3}\right) \quad (1)$$

where Q (Å^{-1}) is the momentum transferred from the neutron to the sample and α_i (Å) is related to a weighted sum of all the displacements of the atom. Thus, not only the energies of the vibrational transitions (the eigenvalues, ν_i) but also the atomic displacements (the eigenvectors, u_i) are available from experimental observation. This significantly enhances the information obtainable from the vibrational spectrum and adds to that from the complementary Raman and infrared vibrational spectroscopic methods, allowing to detect some low frequency modes unavailable to these optical techniques. Since the spectral intensities can be quantitatively compared with those calculated by theoretical methods, by combining the INS results with quantum mechanical molecular orbital calculations it is possible to link molecular geometry with the experimental spectroscopic features, and produce a consistent conformation for the systems under investigation.

The present work reports a conformational study, by vibrational spectroscopy coupled to quantum mechanical calculations (at the density functional theory and plane-wave levels), of chromone and two derivatives displaying a carboxylic moiety in different positions of the heterocyclic ring – chromone-2-carboxylic acid (2CA) and chromone-3-carboxylic acid (3CA) (Fig. 1). In particular, the H-bonding profile of these substituted chromones was investigated, since it is determinant of their antioxidant properties. A complete spectral assignment of the compounds was achieved, since all vibrational spectroscopic techniques were available to this study – FTIR, Raman and INS.

2. Methods and calculations

2.1. Chemicals

Chromone, chromone-2-carboxylic acid, chromone-3-carboxylic acid, deuterated dimethylformamide (DMF-d_7, 99.5%)

and all other reagents and solvents (*pro analysis* grade) were purchased from Sigma–Aldrich Química S.A. (Sintra, Portugal).

Saturated solutions of the chromone derivatives were prepared in DMF-d_7, and stored in the dark (in order to avoid photoinduced oxidation). The spectra were run within a few hours of the preparation of the solutions.

2.2. FTIR spectroscopy

The Fourier transform infrared (FTIR) spectra were recorded in a Bruker Optics Vertex 70 FTIR spectrometer, in the range 4000–400 cm^{-1}, using KBr disks (*ca.* 2% (w/w)), a KBr beamsplitter, and a liquid-nitrogen cooled Mercury Cadmium Telluride (MCT) detector. The FTIR spectra were collected for 60 scans, with a 2 cm^{-1} resolution. The errors in wavenumbers were estimated to be less than 1 cm^{-1}.

2.3. Raman spectroscopy

The Raman spectra were obtained at room temperature, in a triple monochromator Jobin-Yvon T64000 Raman system (focal distance 0.640 m, aperture *f*/7.5) equipped with holographic gratings of 1800 grooves mm^{-1}. The premonochromator stage was used in the subtractive mode. The detection system was a liquid nitrogen cooled non-intensified 1024 × 256 pixel (1") charge coupled device (CCD) chip.

The 514.5 nm line of an Ar^+ laser (Coherent, model Innova 300-05) was used as the excitation radiation, providing *ca.* 50 mW (for the solids) and *ca.* 100 mW (for the solutions) at the sample position. A 90° geometry between the incident radiation and the collecting system was employed. The entrance slit was set to 200 μm, as well as the slit between the premonochromator and the spectrograph. Samples were sealed in Kimax glass capillary tubes of 0.8 mm inner diameter. Under the above mentioned conditions, the error in wavenumbers was estimated to be within 1 cm^{-1}.

2.4. INS spectroscopy

The INS spectra were obtained at the ISIS Pulsed Neutron and Muon Source of the Rutherford Appleton Laboratory (United Kingdom), on the TOSCA spectrometer. This is an indirect geometry time-of-flight, high resolution ($(\Delta E/E)$ *ca.* 2%), broad range spectrometer [5].

Solid compounds (*ca.* 3 g), were wrapped in aluminium foil, while the solutions (4.8–9.6 ml) were placed in thin walled aluminium cans, which filled the beam. The samples were cooled to *ca.* 20 K before collecting the spectra. Data was recorded in the energy range between 4000 and 16 cm^{-1}, and converted to the conventional scattering law, $S(Q,\nu)$ *vs.* energy transfer (in cm^{-1}) through standard programs.

2.5. Quantum mechanical calculations

The quantum mechanical calculations were performed using the Gaussian 03W program [6] within the density functional theory (DFT) approach, in order to properly account for the electron correlation effects (particularly important in this kind of conjugated systems). The widely employed hybrid method denoted by B3LYP, which includes a mixture of HF and DFT exchange terms and the gradient-corrected correlation functional of Lee, Yang and Parr [7,8], as proposed and parameterised by Becke [9,10], was used, along with the double-zeta split valence basis set 6-31G** [11]. The use of diffuse functions was also tested (6-31++G** [12]).

Molecular geometries were fully optimised by the Berny algorithm, using redundant internal coordinates [13]: the bond lengths to within *ca.* 0.1 pm and the bond angles to within *ca.* 0.1°. The final root-mean-square (rms) gradients were always less than 3×10^{-4} hartree $bohr^{-1}$ or hartree $radian^{-1}$. No geometrical constraints were imposed on the molecules under study.

Inclusion of the solvent (DMF) was simulated by performing self-consistent reaction field (SCRF) calculations. A continuum representation – the integral equation formalism (IEF) version [14–16] of Tomasi's polarised continuum model (PCM) [17–19] – was used (applying the united atom topological model). This approach defines the molecular cavity as the union of a series of interlocking spheres, centred on each of the distinct atoms of the molecule. Furthermore, a solvent molecule was explicitly considered in the calculation, in order to account for the probable occurrence of solvent – chromone interactions, through H-type close contacts.

The harmonic vibrational wavenumbers, as well as Raman activities and infrared intensities, were always obtained at the same theory level as the geometry optimisation procedure. As the widely used Merrick et al. [20] scale factors do not adequately reproduce the experimental data in this kind of systems, a new set of scale factors were proposed, leading to a quite good agreement between theoretically predicted and experimental frequencies: four different scaling factors were used – 1.18, in the low wavenumber region (below 175 cm^{-1}); 1.05, in the interval from 175 to 400 cm^{-1}; 0.985, from 400 to 1850 cm^{-1}; and 0.957, above 3000 cm^{-1}.

Furthermore, pK_a values were calculated for the compounds under study, using the VSXC pure DFT approach [21] coupled to the LanL2DZ-ECP (effective core potential) basis set (both implemented in Gaussian 03W), following the protocol proposed by Benson [22] without scaling. Additional PCM optimizations have not been performed, and electronic energies were adjusted only by the ZPE's.

Natural bond order (NBO) calculations were also carried out, in order to determine the stabilising orbital interactions, applying the donor–acceptor viewpoint approach [23], at the B3LYP/6-31G** level. The Gaussian 03W implemented routines [24] were used to convert the DFT molecular orbitals to a set of NBO orbitals corresponding to a hypothetical Lewis structure with strictly localised electron pairs. The NBO calculations were undertaken within the resonance option (from Gaussian), pointed out as the most suitable for NBO studies in this kind of highly unsaturated chemical systems. In the NBO formalism, the electron delocalisation is represented by the off-diagonal terms in the Kohn–Sham matrix, and the subsequent stabilisation energy is calculated by means of the equation

$$E^{(2)} = \Delta E_{ij} = q_i \frac{F(i,j)^2}{\varepsilon_j - \varepsilon_i} \quad (2)$$

where $F(i,j)^2$ is the off-diagonal Fock matrix element between the *i* and *j* (donor and acceptor orbitals, respectively) NBO orbitals, q_i is the donor orbital occupancy, and ε_i and ε_j are the orbital energies from the donor and acceptor orbitals, represented by the diagonal elements of the Fock matrix. In all cases, NLMO (natural localised molecular orbital) bond order calculations were carried out.

Plane-wave calculations were performed, based on density functional theory methods within the Perdew–Zunger [25] local density approximation (LDA), and plane wave expansions, as implemented in the PWSCF code from the Quantum Espresso package [26], were used. The atomic coordinates were fully optimised, starting from the isolated-molecule structures of both the chromone moiety and its dimers, designed with the Avogadro graphical interface. The molecules were placed in a cubic box with a 30-bohr length, to ensure negligible interactions with their periodic images. The pseudopotentials employed were of the norm-conserving type – a von Barth–Car [27] approach was applied to the H and C atoms, and a Martins–Troullier [28] type was used for the O atoms.

Table 1
Calculated relative energies (kJ mol^{-1}) for the distinct conformers found for 2CA and 3CA.

	2CA				3CA			
	2CA-1[a]	2CA-2	2CA-3	2CA-4	3CA-1	3CA-2	3CA-3	3CA-4
Isolated molecule Gaussian[b]	0[c]; 4.5[d]	1.3; 1.8	8.6; 6.1	27.5; 3.0	0; 7.3	28.5; 3.5	34.1; 5.0	65.0; 7.1
DMF solution[e]	0; 6.7	1.2; 2.7	13.8; 8.7	25.8; 3.6	0; 9.9	12.8; 4.7	14.1; 7.3	36.2; 10.0
Isolated molecule	0		7.7		0	52.0		
Plane wave[f]								

[a] According to Fig. S1.
[b] At the B3LYP/6-31G** level.
[c] Using the zero-point vibrational energy correction; final energy scaled by a factor of 0.9806 [20].
[d] Total calculated dipole moment, 1D = 1/3 × 10^{-2} cm.
[e] At the B3LYP/6-31G** level, using the IEF-PCM approach within the SCRF theory.
[f] At the LDA/PWSCF level.

This choice of methods has been guided by the fact that Raman activities can only be calculated with PWSCF methods, using a LDA DFT approach and norm-conserving pseudopotentials. A cut-off energy of 70 Ry and a Monkhorst–Pack grid [29] of 1 × 1 × 1 were found sufficient to attain convergence. The dynamical matrix was calculated for the optimised geometries within the DFT Theory [30], and was diagonalised to obtain the vibrational normal mode wavenumbers, as well as the Raman activities, S_i. The latter, straightforwardly derived from the program output, cannot be compared directly with the experiment, the expression relating the Raman differential scattering cross section with the Raman activity being [31],

$$\frac{\partial\sigma_i}{\partial\Omega} = \frac{(2\pi)^4}{45}(\nu_0 - \nu_i)^4 \frac{h}{8\pi^2 c\nu_i B_i} S_i. \quad (3)$$

where h, k, c and T represent the Planck and Boltzmann constants, the speed of light and the temperature (in K), respectively; ν_0 and ν_i stand for the frequency of the laser excitation, and the normal mode frequencies; and B_i is a temperature factor, set to 1. The frequency of the laser excitation, for a 514.5 nm line of an Ar^+ laser, was considered to be 19,436 cm^{-1}. The theoretical Raman intensity was calculated according to

$$I = C(\nu_0 - \nu_i)^4 \frac{S_i}{\nu_i} \quad (4)$$

C being a constant. In order to simulate the line width of the experimental lines, an artificial Lorentzian broadening was introduced using the SWizard program (revision 4.6) [32,33]. The band half-widths were considered to be equal to 10 cm^{-1}.

The theoretical INS transition intensities were obtained from the calculated normal mode eigenvectors and the spectra simulated using the dedicated aCLIMAX program [34]. For isolated molecule calculations, this program accomodates the impact of the external modes of extended molecular solids through the choice of a suitable value for α_i (Eq. (1)).

3. Results and discussion

3.1. Conformational analysis

According to the theoretical calculations presently performed, the chromone molecule (C) has only one possible stable geometry at room temperature (Fig. 1), while for its carboxylic derivatives 2CA and 3CA four distinct conformers were obtained (Fig. S1, Supplementary material). These are interconvertible upon internal rotation around the C_2–C_9 and C_9–O_{10} bonds, corresponding to different orientations of the carboxylic group relative to the chromone skeleton, and to either an *s-trans* or an *s-cis* orientation of the carboxylic moiety. For all three compounds, the lowest energy species display a planar structure, the carboxylic group being coplanar with the chromone skeleton. For 2CA, the most stable geometry was found to be that with a *syn* orientation of the two carbonyl moieties and an *s-cis* conformation of the carboxylic group (Fig. 1). For the 3-carboxylic derivative, in turn, the 3CA-1 minimum displays an *s-trans* orientation, allowing a highly favoured intramolecular H-bond between the ketonic carbonyl and the carboxylic hydroxyl ($(O_{10})H\cdots O_{12}(=C)$, d = 171 pm, Fig. 1). Actually, this is the only species expected to occur at room temperature since the next calculated conformers correspond to very high relative energies (ΔE = 28.5, 34.1 and 65.0 kJ mol^{-1}, Table 1). Furthermore, this preferred intramolecular $(O_{10})H\cdots O_{12}(=C)$ close contact justifies the abnormally high pK_a value reported for 3CA – 8.85 [35] as compared to 2.55 [36] for the 2-carboxylic analogue, for which no such interaction is possible. These pK_a values were presently confirmed by DFT calculations: 8.59 and 2.04 were obtained for the most stable conformers of 3CA and 2CA, respectively.

The plane wave (PW) calculations carried out for these systems allowed to verify the occurrence of stable dimeric species in the condensed phase, both centrosymmetric and non-centrosymmetric (Fig. 2). This can justify the higher stability of geometry 2CA-1, as compared to the third most stable form 2CA-3 (ΔE = 7.7 kJ mol^{-1}, Table 1) which allows the formation of a $(O_{10})H\cdots O_1$ close contact (Fig. S1, Supplementary material). The occurrence of this hydrogen bond is unfavoured relative to the formation of the centrosymmetric dimer ($2CA_c$, Fig. 2), the former being a medium to weak interaction (d = 203 pm, yielding a five-membered intramolecular ring) while the latter involves two strong top-to-top $(O_{10})H\cdots(O_{11})H$-bonds (d = 142 pm).

Inclusion of diffuse functions (in both the heavy atoms and the hydrogens) did not significantly affect either the relative conformational energies of the compounds or the agreement between their predicted and experimental vibrational spectra. In fact, for this kind of unsaturated, heterocyclic systems displaying intramolecular H-bonds, DFT methodologies (including B3LYP with any type of basis set), even considering both polarisation and diffuse functions, cannot fully describe this type of close contacts, which are often determinant of the conformational equilibrium. This is due to the ineffective representation of dispersive interactions [37], leading to an underestimation of weak H-bonds (of dispersive nature) [38] such as the one present in conformer 2CA-3. On the other hand, it is well known that the 6-31G* basis set, within a DFT approach, overestimates strong (electrostatic) intramolecular H-type interactions [39]. Indeed, these are quite well represented through the PW method, which predicts a much higher energy gap between the 3CA-1 and 3CA-2 species (ΔE = 52.0 *vs.* 28.5 kJ mol^{-1}, Table 1 and Fig. 1).

Solvation of the molecules – using DMF as a suitable solvent for these compounds – predicted no appreciable influence on their main conformational preferences, despite the slight variation observed in the relative energies, namely for the 3-carboxylic derivative, for which the 3CA-2 geometry was favoured in solution (ΔE = 12.8 kJ mol^{-1}, 0.6% population) as compared to the gas

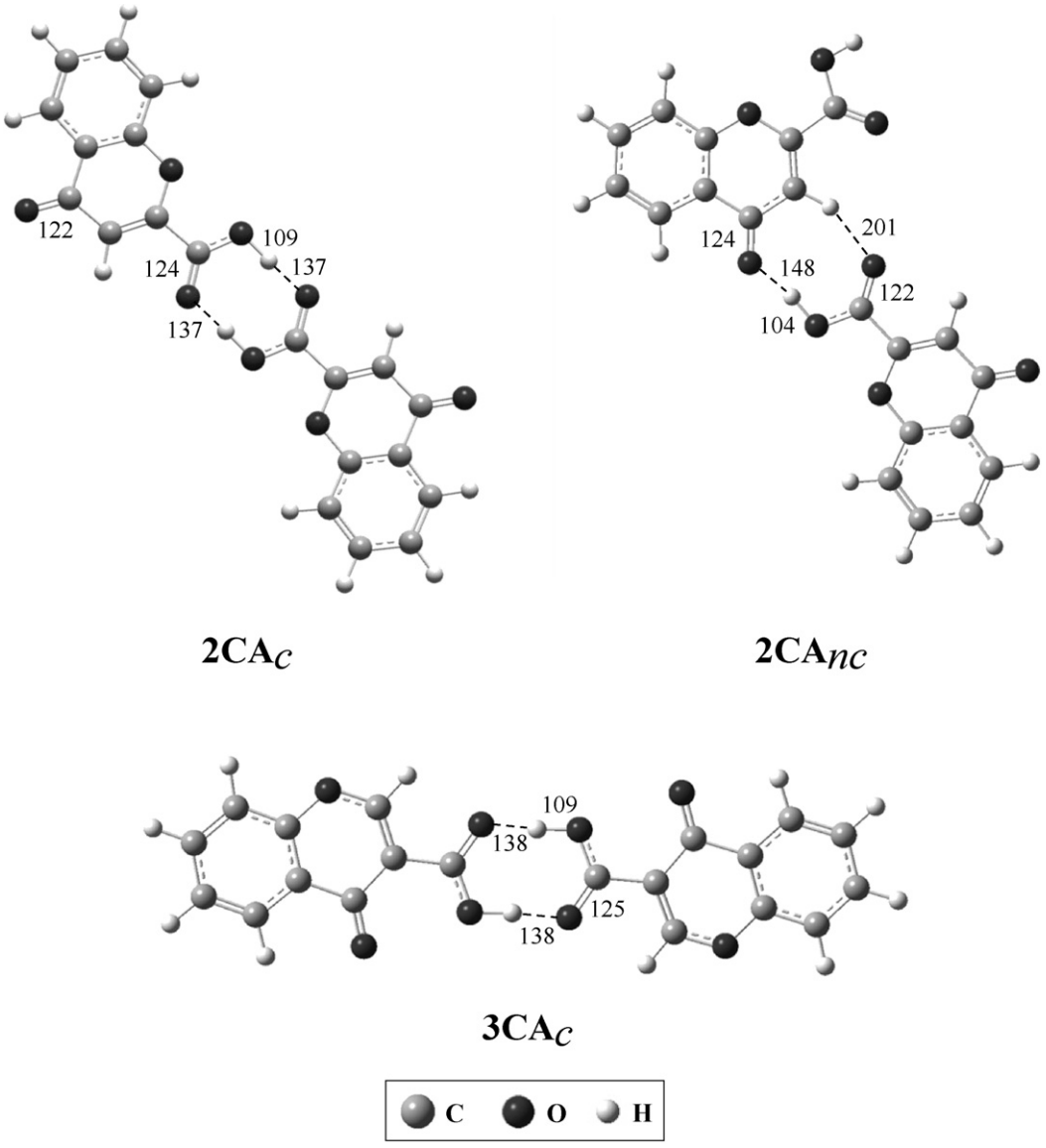

Fig. 2. Calculated (LDA/PWSCF) structures for dimeric species of the chromone carboxylic derivatives 2CA and 3CA – (*c*) centrosymmetric; (*nc*) non-centrosymmetric (distances are in pm).

phase (ΔE = 28.5 kJ mol^{-1}, 0.0% population) (Table 1). This may be explained by the possibility of occurrence of H-bond type interactions between the carboxylic moiety of the molecule and the solvent – (O)H···O$_{(\text{from DMF})}$ – that will stabilise the geometry lacking the intramolecular (O$_{10}$)H···O$_{12}$(=C) close contact – 3CA-2, otherwise largely unfavoured relative to the 3CA-1 species.

NBO (natural bond order) calculations were performed for the different conformers of 2-carboxylic and 3-carboxylic acid chromones, in order to assess the key stabilising electronic delocalisations in this kind of systems and to compare the dynamics of these interactions for the different positions of the carboxylic group. In 3CA, besides the electronic delocalisations related to the π system of the aromatic ring, common to both conformers, the key interaction is the delocalisation between the carbonyl group and the C$_2$=C$_3$ double bond. For 3CA-1 a stabilisation energy of 571.79 kJ mol^{-1} is associated with the π^*(C$_4$=O$_{12}$) to π^*(C$_2$=C$_3$) delocalisation, while for 3CA-2 the conformational stability is mainly due to the π^*(C$_2$=C$_3$) to π^*(C$_4$=O$_{12}$) interaction (448.15 kJ mol^{-1}). These large energy values are mainly due to the small energy gaps between the involved orbitals (0.01325 a.u. for 3CA-1 and 0.01310 a.u. for 3CA-2), which reflect the degenerated character of the interacting orbitals (donor and acceptor). The different stabilising energies for each conformer can be understood through different donor orbital occupancies (q_i): 0.2891 is the π^*(C$_4$=O$_{12}$) occupancy value in 3CA-1, whereas 0.1981 is the corresponding value for π^*(C$_2$=C$_3$) in 3CA-2. The donor orbital occupancy is a multiplier in Eq. (2) (Section 2), thus leading to an increase in the delocalisation energy for larger occupancy values.

These delocalisations, as well as those involved in the aromatic ring π currents, occur between π^* orbitals with a small but detectable occupancy, representing molecular orbital deviations from the idealised Lewis structure due to intrinsic hyperconjugation, and can be regarded as "native molecular delocalisations" [40]. In addition, interaction between these π^* orbitals yields very strong electronic delocalisations, that can attain quite high energy values thanks to the proximity between the orbital energy levels, expected when dealing with orbitals of the same type (π^*).

The π^*(C$_2$=C$_3$) to π^*(C$_9$=O$_{11}$) delocalisation is the second most important factor in 3CA-1 (the aromatic ring π currents having been omitted for simplicity): 306.44 kJ mol^{-1} as compared to

2.092 kJ mol^{-1} for 3CA-2. Indeed for a similar occupancy of the donor orbital in both conformers (0.1982 for 3CA-2 *vs.* 0.1967 for 3CA-1) and a much smaller energy gap in 3CA-2 (0.0020 a.u. for 3CA-2 *vs.* 0.0196 a.u. for 3CA-1), it can be presumed that the off diagonal element $F(i, j)^2$ (Eq. (2)) should be null for 3CA-2, corresponding to no delocalisation at all between these orbitals ($\pi^*(C_2{=}C_3)$ to $\pi^*(C_9{=}O_{11})$).

The third most important delocalisation in these compounds, from the O_{10} p-rich lone pair ($LP(O_{10})$) to $\pi^*(C_9{=}O_{11})$ presents comparable values for the two conformers (230.37 kJ mol^{-1} for 3CA-1 *vs.* 213.72 kJ mol^{-1} for 3CA-2), reflecting a similar mechanism for this process as well as an analogy between the intervening orbitals in both conformers.

This NBO donor–acceptor analysis shows that the charge transfer from the carbonyl group in conformer 3CA-1 leads to a certain degree of single bond character in this moiety, with a NLMO (natural localised molecular orbital) bond order of 1.2463, comparable to that of the C_9–O_{10} bond (0.7861), which may explain the abnormally low experimental frequency for the ($C_4{=}O_{12}$) stretching mode observed for 3CA (1631 cm^{-1}, Table 2). On the other hand, for conformer 3CA-2 the electronic density of the $C_4{=}O_{12}$ bond is larger (bond order equal to 1.3501), thus leading to a higher predicted wavenumber for $\nu_{C=O}$ (1736 cm^{-1}, Table 2). Such a band is not detected by Raman spectroscopy, as expected (since conformer 3CA-1 is the main species present in the solid, at room temperature).

The NLMO calculations also enable to identify the difference between the O_{10}—H_{20} bond orders in each of the 3CA most stable geometries: 0.4094 in 3CA-1 from a total bond order of 0.5449 for the hydrogen (H_{20}) atom, and 0.4712 in 3CA-2 from a total of 0.5125. This fact reflects some delocalisation character of the H_{20} atom in 3CA-1, its bonding being distributed within the molecule, mainly to the O_{12} carbonylic oxygen (only 75% being related to the carboxylic O_{10}). On the other hand, for 3CA-2 92% of the H_{20} bond order refers to O_{10}–H_{20}, other interactions being almost negligible.

The NBO calculations performed for the most stable conformer of the 2CA derivative (2CA-1) clearly allow to conclude that the three major stabilising delocalisations involve the carboxylic acid group. The largest, $\pi^*(C_9{=}O_{11})$ to $\pi^*(C_2{=}C_3)$, leads to a stabilisation energy of 233.80 kJ mol^{-1}, which is only 16.23 kJ mol^{-1} lower than the corresponding one for the 2CA-2 species (Fig. S1). This difference is probably due to the *anti* configuration of the double bonds in the latter case. The next two relevant interactions arise from the delocalisations between p-rich lone pairs and the carboxylic acid anti-ligand orbitals: (i) O_{11} lone pair to $\sigma^*(C_9{-}O_{10})$ – 136.98 kJ mol^{-1} (3.93 kJ mol^{-1} lower relative to 2CA-2) and (ii) O_{10} lone pair to $\pi^*(C_9{=}O_{11})$ – 207.36 kJ mol^{-1} (8.45 kJ mol^{-1} higher relative to 2CA-2).

For the most stable *s-trans* conformer (2CA-3, Fig. S1), the ruling delocalisations are identical, with the exception of the $\pi^*(C_9{=}O_{11})$ to $\pi^*(C_2{=}C_3)$ interaction, reaching a predicted energy of 411.75 kJ mol^{-1}, almost double relative to 2CA-1. This difference is completely justified by the distinct energy gaps between the intervening orbitals (2.02-fold in 2CA-1 relative to 2CA-3).

Finally, by comparing the NLMO bond orders of the distinct 2CA conformers, a similarity between the various bonds is perceptible, with a single minor difference in the O_{10}—H_{20} bond order: *ca.* 0.465 for the *s-cis* conformers, 0.466 for 2CA-3 and 0.477 for 2CA-4 (Fig. S1). This allows to conclude that there is no evidence of formation of a $H_{20}\cdots O_1$ hydrogen bond in 2CA-3.

Comparing 3CA to 2CA, the first fact that stands out is that for the latter the electronic delocalisations are much less dependent on molecular conformation. The most significant interactions obtained for the *s-cis* 2-substituted derivative lie within the same range for all conformers, and therefore they are not responsible for the corresponding conformational preferences. For the *s-trans* geometries, in turn, the electronic delocalisations involving the carboxylic group, although qualitatively the same, have more significant energy differences. Regarding 3CA, the most important delocalisations refer to π^*–π^* interactions, the largest being those related to the π aromatic ring currents.

The NBO analysis revealed that electronic delocalisations involving $\pi^*(C_4{=}O_{12})$ orbitals are determinant for 3CA stability, namely governing the energy difference between conformers 3CA-1 and 3CA-2. In turn, for 2CA the interactions associated to the carboxylic moiety are the most relevant. It was verified that changing the position of the carboxylic acid in the chromone skeleton greatly alters the dynamics of stabilising electronic delocalisations. For the 3-carboxylic chromone, the proximity between the ($C_4{=}O_{12}$) ketonic and carboxylic groups is the ruling feature for the molecule's stabilisation.

3.2. Vibrational analysis

3.2.1. Raman and infrared

The solid state experimental Raman data for chromone and its 2-carboxylic derivative, in the solid state, is comprised in Fig. 3, and that for 3CA is depicted in Fig. 4(A). Fig. 4(B) represents the theoretically predicted Raman spectra for the two 3CA conformers: 3CA-1 (most stable, *s-trans* species) and 3CA-2 (*s-cis*). As previously discussed, the *s-trans* geometry displays a highly favoured $(O_{10})H\cdots O_{12}$ interaction (d = 171 pm, Fig. 1), yielding a stable six-membered intramolecular ring (planar), while the *s-cis* orientation of the carboxylic moiety in the 3CA-2 species hinders this type of close contact, giving way to intermolecular H-bonds in the condensed phase (formation of dimers). These conformational preferences are clearly reflected in the theoretically predicted Raman pattern: for 3CA-1 no isolated band was detected for the out-of-plane deformation of the carboxylic OH group (γ_{OH}), due to its involvement in the intramolecular H-bond, while for 3CA-2 both out-of-plane (γ_{OH}) and in-plane (δ_{OH}) modes were observed, at 617 cm^{-1} and 1232 cm^{-1} respectively (Fig. 4(B) and Table 2). Moreover, δ_{OH} was found to be shifted to high frequency in 3CA-1 as compared to 3CA-2 (1283 cm^{-1} *vs.* 1232 cm^{-1}), similarly to the deformation of the carboxylic moiety ($\Delta(O_{10}C_9O_{11})$, 726 cm^{-1} *vs.* 698 cm^{-1}), much as expected in the light of the OH participation in a medium-to-strong H-type interaction. Also, the stretching of the ketonic carbonyl ($C_4{=}O$) suffered a quite large shift to low frequency upon H-bond formation: 1736 cm^{-1} for 3CA-2 *vs.* 1673 cm^{-1} for 3CA-1. The carboxylic $\nu_{C=O}$ oscillator, in turn, displays an opposite shift, being detected at a higher wavenumber for the *s-trans* geometry, comprising a $(O_{10})H\cdots O_{12}(=C)$ close contact, as compared to the *s-cis* one – 1818 cm^{-1} *vs.* 1774 cm^{-1} (Fig. 4(B)). This may be explained by the electronic delocalisation occurring from the ketonic carbonyl ($C_4{=}O_{12}$) to the carboxylic $C_9{=}O_{11}$ group upon formation of the intramolecular H-bond. This will lead to a force constant decrease of the $C_4{=}O_{12}$ oscillator coupled to a force constant increase of the $C_9{=}O_{11}$ one. This redistribution of the electronic density may also be the basis of the much lower intensity predicted for the $C_2{=}C_3$ stretching band (at 1592 cm^{-1}) in 3CA-1 as compared to 3CA-2 (Fig. 4(B)).

The Raman experimental pattern agrees well with these findings (Figs. 3 and 4(A), Tables 2–4). In fact, the ketonic $\nu_{C=O}$ mode has a much higher intensity for 2CA (at 1629 cm^{-1}) as compared to 3CA (where it is hardly detected at 1631 cm^{-1}, Fig. 4(A)) as a consequence of the $(O_{10})H\cdots O_{12}(=C)$ interaction that causes a significant variation in the polarizability of this particular oscillator. In addition, while for 2CA there is only one $\nu_{C=O}$ feature assigned to the carboxylic moiety (at 1739 cm^{-1}), two such modes are observed for 3CA possibly due to the coexistence of two species in the condensed phase: a monomeric one displaying the favoured

Table 2
Experimental and calculated vibrational wavenumbers (cm^{-1}) for conformers 1 and 2 of chromone-3-carboxylic acid (3CA).

Experimental				Calculated				Approximate description[a]
FTIR	Raman	INS		B3LYP[b]	B3LYP – conformer 2[b]	PW[c]	PW (3CA*c*)	
		Solid	DMF-d_7 sol.					
					3585			ν (OH)$_{monomer}$
2637				3158		2667		$\nu\nu$(OH)$^{intramolec\ bond}_{monomer}$
3138	3133			3108	3104	3132	3110	ν (C_2H)
3080	3083 sh			3088	3085	3141	3123	ϕ 2 + ϕ 7a + ϕ 20a + ϕ 13
	3073			3085	3082	3124	3115	
				3072	3069	3134	3105	
				3060	3057	3117	3094	
							2562, 2341	ν (OH)$_{dimer}$
1744	1759			1818	1774	1765		ν (C_9O_{11})
	1739						1645	ν (C_9O_{11})
1621	1631 sh			1673	1736	1596	1750	ν (C_4O_{12})
1615	1614			1643	1642	1643	1565	ϕ 8a
1577	1575			1625	1630	1638	1550	ϕ 8a + ν (C_2C_3) + ν (C_4O_{12})
1569							1571	δ (O_{10}H)$_{bonded}$
1560	1561 sh			1592	1592	1586	1513	ϕ 8a/ϕ 8b + υ (C_2C_3)
				1496	1488	1478		ϕ 19b + δ (O_{10}H)
1486	1488			1483	1480	1460		ϕ 19a + δ (O_{10}H)
1470 sh	1470 sh						1454	δ (O_{10}H)$_{bonded}$
1460 sh	1461	1470	1471	1469	1402	1521		δ (O_{10}H)
1443	1445			1405	1383	1403	1439	ν (C_9O_{11}) + δ (C_2H) + δ (O_{10}H)
1403	1404	1406		1364	1361	1297	1422	ϕ 14 + δ (C_2H)
1349	1353	1351				1276	1343	δ (C_2H)
1317	1319	1324		1317	1322	1244	1335	δ (C_2H) + ϕ 3
1272	1276	1276		1283	1232	1244	1317	δ (OH) + δ (C_2H) + ν (C_3C_9) + ϕ 3
1255	1255	1261		1267	1268	1220	1313	ϕ 3 + δ (C_2H)
1212	1212	1216		1218	1195	1172	1218	ϕ 9b + ν ($C_{8a}O_1$) + ν ($C_{4a}C_4$)
1176	1175	1184		1181	1176	1140	1155	ϕ 9a + ν ($C_{8a}O_1$) + ν (C_2O_1)
1147	1148	1152		1161	1158	1130	1123	ϕ 15 + δ (O_{10}H)
1122	1122	1129	1130	1135	1125	1093	1105	ϕ 15 + ν (C_2O_1) + ν (C_9O_{11})
	1108	1107						ν (C_9O_{10})$_{bonded}$
1095 sh	1098	1095	1090	1104	1100	1026	1088	ϕ 9b + δ (C_2H)
1023	1026	1030		1036	1037		1049	ϕ 1
1009	1007	1012		993	991	992	972	ϕ 17b/ϕ 17a
981	980			967	964	960	942	ϕ 17a
967	965	978		960	966	943	936	γ (C_2H)
931	930	935	933	927	910	938	905	ϕ 12 + Δ ($C_4C_3C_2$)
894	885	885	897	853	617	1032	1134	γ (OH)
875			875	877	878	874	901	ϕ_{oop}
853	853	856	854	849	848	847	857	ϕ 12
816	814	818		793	806	816	825	ϕ 10b + Γ ($C_{4a}C_4C_3$)
774	780	784	767	769	773	763	802	ϕ 11
757	753	756		756	753	758	784	ϕ 6a + Δ ($O_1C_2C_3$)
751				730	752	753	755	ϕ 4 + Γ ($O_{11}C_9O_{10}$)
729	731	734		726	698	734	728	Δ ($O_{11}C_9O_{10}$) + ϕ 6a
682		685		669	690	682	676	ϕ 4 + Γ ($O_{11}C_9O_{10}$) + Γ ($C_{4a}C_4C_3$)
641	640	640		641	637	638	649	ϕ 6a + Δ ($O_{12}C_4C_3$) + Δ ($C_3C_9O_{11}$)
575	575	576		570	563	577	587	Δ ($C_{4a}C_{8a}O_1$) + Δ ($O_{11}C_9O_{10}$)
549	548	547		545	543	553	547	ϕ 16b + Γ ($C_{8a}O_1C_2$)
537	536			537	533	541	526	ϕ 6b + Δ ($C_2C_3C_9$)
495	494	495		494	489	494	486	ϕ 6b + Δ ($C_{4a}C_4O_3$)
465	461	464		462	463	464	455	ϕ 16a + Γ ($O_1C_2C_3$)
435	437	438		426	411	436	444	Δ ($C_3C_9O_{10}$) + Δ ($C_{4a}C_4O_{12}$)
422	418	422		415	413	417	406	ϕ 16a + Γ ($O_1C_2C_3$) + γ (C_2H)
	359	359		365	326	380	392	Skeletal modes
	325	324	313	334	338	311	319	Skeletal modes
	270	277	299	276	276	260	268	Γ ($C_{8a}O_1C_2$) + Γ ($C_4C_3C_2$)
	251	255		245	242	231	235	Skeletal modes
		242						External mode
			221		221[d]			DMF (τ(CD_3))[d]
	200	202		202		195	225	ν (OH···O)
	175	176	174	177	159	154	131	Skeletal modes
			136		143[d]			ν ($OH_{3CA}\cdots O_{DMF}$)[d]
	128	119	118					External mode
		110	110	112	67	102	98	Γ ($O_{10}C_9O_{11}$)
		100	99					External mode
		73	74	77	44	72	74	Skeletal modes
		60	56					External mode

[a] Atoms are numbered according to Fig. 1. The Wilson notation was used for the description of benzene derivatives normal vibrations (ϕ) [41,42]; for in-plane vibrations: C–C stretching vibrations (8a, 8b, 14, 19a, 19b), C–H/X bending vibrations (3, 18a, 18b), radial skeletal vibrations (1, 6a, 6b, 12) C–H stretching vibrations (2, 20a, 20b, 7a, 7b); for out-of-plane vibrations: C–H/X vibrations (5, 10a, 11, 17a, 17b), skeletal vibrations (4, 16a, 16b). δ – in-plane deformation, ν – stretching mode, γ – out-of-plane deformation, Δ – in-plane skeletal deformation, Γ – out-of-plane skeletal deformation. sh – shoulder. Subscripts: oop – out of plane.

[b] At the B3LYP/6-31G** level; wavenumbers are scaled according to Merrick et al. [20].

[c] For 3CA-1 monomer (Fig. 1), at the LDA/PWSCF level.

[d] Solvent interaction with 3CA. Calculated at the B3LYP/6-31G** level, considering DMF-d_7 as the solvent within the SCF-SCRF approach, and an explicitly added DMF molecule.

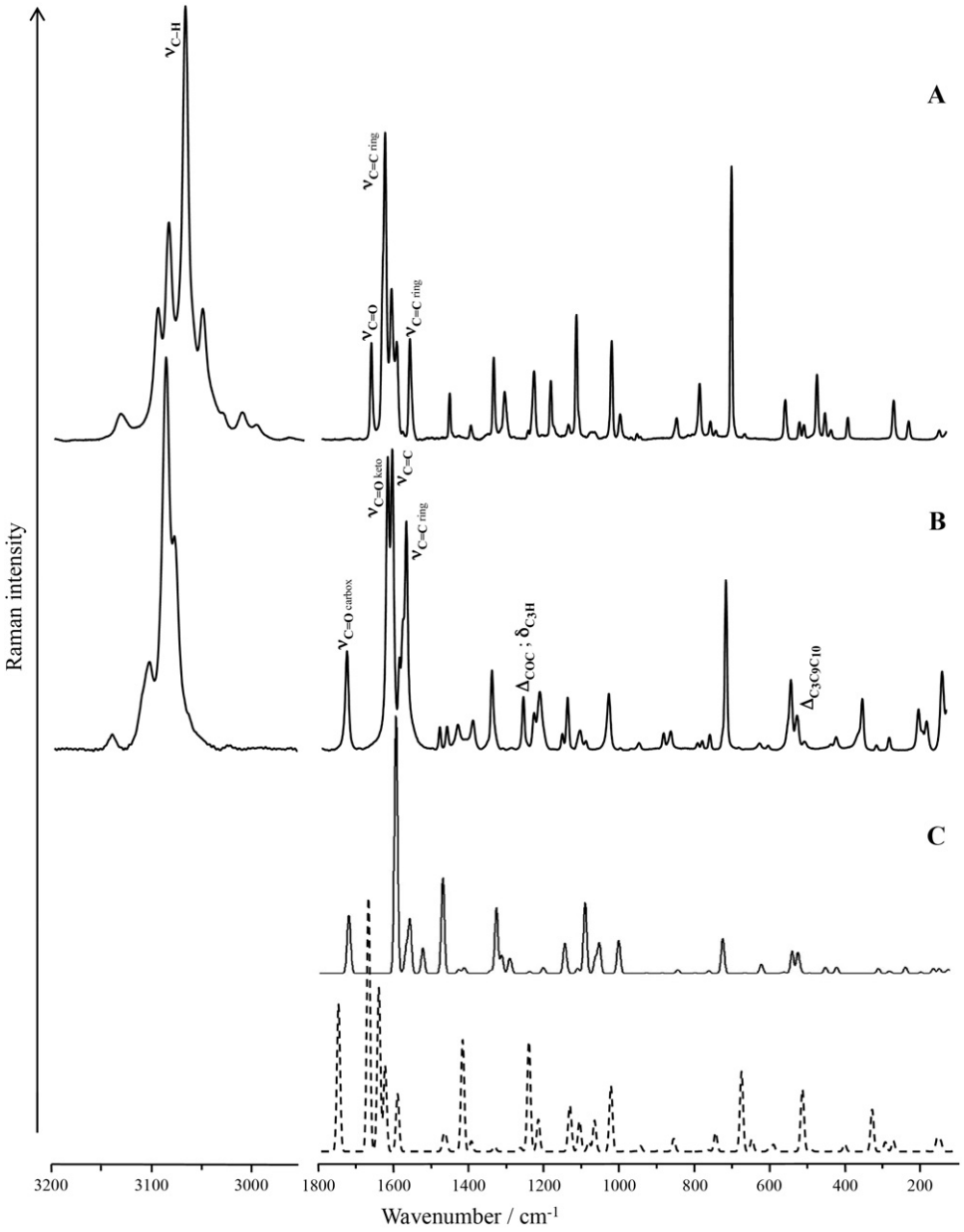

Fig. 3. Experimental Raman spectra (100–1800 and 2950–3200 cm^{-1}; solid state, 25 °C) for chromone (A) and 2CA (B). (C) Calculated (LDA/PWSCF) spectra for 2CA monomer (dotted line) and 2CA centrosymmetric dimer (solid line) (the atoms are numbered according to Fig. 1).

intramolecular H-bond ($\nu_{C=O}$ at 1759 cm^{-1}), and a dimeric species due to the formation of an intermolecular interaction (top-to-top (O)H···O(=C), $\nu_{C=O}$ at 1739 cm^{-1}). The very low calculated values for the hydroxyl stretching modes when considering the 2CA stable dimeric species (Table 4) are due to the considerable overestimation of the intermolecular H-type interactions by the LDA methodology. Furthermore, 2CA displays only one carboxylic deformation mode (at 715 cm^{-1}, Fig. 3), while for 3CA both the ($O_{11}C_9O_{10}$) in-plane and out-of-plane deformations are observed (at 731 and 753 cm^{-1}, respectively, Fig. 4).

The infrared profiles obtained for chromone and its 2- and 3-carboxylic derivatives (Tables 2–4) are in total agreement with the previously described conformational behaviour.

3.2.2. Inelastic neutron scattering

INS spectra were obtained for both hydrogenated and O-deuterated solids, as well as for solutions (in DMF-d_7), leading to the detection of the vibrational modes associated to (O—H···O) close contacts, both intra- and intermolecular (in the low wavenumber region). The solid samples yielded very good quality spectra (Fig. 5), allowing to identify the main vibrational bands of the molecules.

As expected, deuteration of the compounds affected the corresponding vibrational pattern according to two main factors: (i) increase in the mass of the oscillators involving the deuterated hydroxyl group and (ii) disruption of the (O_{10})H···O_{12}(=C) interaction (Fig. 1), giving rise to a significantly weaker (O_{10})D···O_{12}(=C) close contact. This was clearly verified for 3CA, for which the INS pattern showed some marked differences upon deuteration as compared to the non-deuterated sample (Fig. 5), consistent with the conformational changes resulting from the break of the intramolecular H-bond between the ketone and the carboxylic moieties, corresponding to a 3CA-1 to 3CA-2 rearrangement (Fig. 1). In fact, the INS stretching band assigned to the intramolecular (OH···O) close contact (at 202 cm^{-1}) decreased considerably upon

Table 3
Experimental and calculated vibrational wavenumbers (cm^{-1}) for chromone (C).

Experimental			Calculated[a]	Approximate description[b]
FTIR	Raman	INS		
3133	3134			(1566 × 2)
3096	3097		3101	ν ($C_3H/C_2H)_{iph}$
			3083	ν ($C_3H/C_2H)_{oph}$ + ϕ 2
3085	3086		3082	ϕ 2 + ν ($C_3H/C_2H)_{oph}$
			3079	ϕ 20a
3070	3069		3067	ϕ 7a
3052	3052		3054	ϕ 13
3012	3013			(1346 + 1670)
	2920			(1462 × 2)
1652	1670		1729	ν (C_4O_{12})
	1631		1648	ν (C_2C_3)
1616	1616		1640	ν (C_2C_3) + ϕ 8a/ϕ 8b
	1602			FR ((718 + 863) + 1567)
1566	1567		1598	ϕ 8b
1475			1489	ϕ 19a
1462	1462	1463	1482	ϕ 19b
1405	1406	1406	1413	δ (C_2H/C_3H) + ν (C_3C_4)
1346	1346		1363	ϕ 14 + δ (C_2H)
1318	1317	1316	1329	ϕ 14/ϕ 3 + ν_{as} (COC) + δ (C_2H)
1256	1255	1252	1267	ϕ3 + δ (C_2H/C_3H) + ν_{as} (COC)
1235	1239		1247	ϕ_{ip} + δ (C_3H) + ν (C_4C_{4a})
1191	1195	1192	1201	ϕ_{ip} + ν (O_1C_{8a}) + δ (C_2H/C_3H)
1147	1148	1151	1159	ϕ 15
1127	1128	1129	1132	ϕ 9b + δ (C_3H)
1077		1084	1083	ϕ 12 + δ (C_3H)
1036	1034	1040	1046	ϕ 18b + δ (C_2H/C_3H) + ν (O_1C_2)
1011	1012	1014	1019	ϕ 1 + δ (C_2H/C_3H) + ν (O_1C_2)
984	983	976	988	ϕ 5
969	967		962	ϕ 17a
957	958		954	γ ($C_2H/C_3H)_{oph}$
864	863	868	875	ϕ 10a
			858	Δ ($C_2O_1C_{8a}$) + ϕ_{ip}
835	833	838	837	γ ($C_2H/C_3H)_{oph}$ + Γ ($C_3C_4C_{4a}$)
801	802	804	803	Δ ($C_2C_3C_4$) + ϕ_{ip}
776	774	778	778	ϕ 11 + γ ($C_2H/C_3H)_{iph}$
758	759	759	759	ϕ 10b + γ ($C_2H/C_3H)_{iph}$
716	718	717	717	ϕ 6a
680	683	681	676	ϕ 4 + Γ ($C_3C_4C_{4a}$)
573	576	574	572	ϕ 6a + Δ ($O_{12}C_4C_3$)
538	537	538	538	ϕ 16b + Γ ($C_2O_1C_{8a}$)
527	527	527 sh	526	ϕ 6b + Δ ($O_{12}C_4C_3$)
491	491	492	488	Δ ($C_4C_{4a}C_{8a}$)
470	470	469 sh	464	Δ ($C_2O_1C_{8a}$) + Δ ($C_3C_4O_{12}$)
461	454	460	462	ϕ 16b + Γ ($C_3C_2O_1$)
404	410	403	400	ϕ 16b + Γ ($C_3C_2O_1$)
	289	289	289	Δ ($C_4C_{4a}C_5$)
	249	247	246	Skeletal mode
	169	177	160	Skeletal mode
		154		External mode
		146		External mode
		113	119	Skeletal mode
		81		External mode
		69		External mode
		51		External mode
		44		External mode
		41		External mode

[a] At the B3LYP/6-31G** level; wavenumbers are scaled according to Merrick et al. [20].
[b] Atoms are numbered according to Fig. 1. The Wilson notation was used for the description of benzene derivatives normal vibrations (ϕ) [41,42]; for in-plane vibrations: C–C stretching vibrations (8a, 8b, 14, 19a, 19b), C–H/X bending vibrations (3, 18a, 18b), radial skeletal vibrations (1, 6a, 6b, 12) C–H stretching vibrations (2, 20a, 20b, 7a, 7b); for out-of-plane vibrations: C–H/X vibrations (5, 10a, 11, 17a, 17b), skeletal vibrations (4, 16a, 16b). sh – shoulder. δ – in-plane deformation, ν – stretching mode, γ – out-of-plane deformation, Δ – in-plane skeletal deformation, Γ – out-of-plane skeletal deformation. Subscripts: ip – in plane, iph – in phase, oph – out of phase. FR – Fermi resonance.

O-deuteration. Indeed, for a total deuteration this band should disappear completely. However, this was hampered by poor water solubility coupled to a high pK_a value (8.85). Several features assigned to skeletal modes prone to be influenced by this interaction (*i.e.* associated to the ($O_{12}C_4C_3C_9O_{10}H$) intramolecular ring) were found to undergo changes upon deuteration: the bands at 325, 359 and 494 cm^{-1}, due to in-plane skeletal deformations (*e.g.* $\Delta(C_3C_9O_{10})$ and $\Delta(C_4C_3C_9)$), displayed a significantly lower intensity in the deuterated compound (Fig. 5). Similarly, a very strong intensity decrease was observed for the two signals at 575 and 640 cm^{-1}, assigned to in-plane and out-of-plane ($C_4C_3C_9$), ($C_3C_9O_{10}$) and ($C_9O_{10}H$) deformations, which were hardly detected in the deuterated sample owing to the D for H substitution. Furthermore, the δ_{OH} mode, detected at 1470 cm^{-1} (as predicted

Table 4
Experimental and calculated vibrational wavenumbers (cm^{-1}) for conformer 1 of chromone-2-carboxylic acid (2CA).

Experimental				Calculated			Approximate description[a]
FTIR	INS		Raman	B3LYP[b]	PW[c]	PW ($2CA_c$)	
	Solid	DMF-d_7 sol.					
				3595	3579		ν (OH)
							(1589 × 2)
			3148	–			(1579 × 2)
			3111	3112	3144	3153	ν (C_3H)
			3094	3084	3138	3136	ϕ 2
				3081	3129	3129	ϕ 20a
3080			3085	3069	3119	3117	ϕ 7a
				3056	3112	3111	ϕ 13
2870 vb						2084	ν $(OH)_{bonded}$
2550 vb						1924	ν $(OH)_{bonded}$
1728			1739	1806	1753	1688	ν (C_9O_{11})
1631			1629	1725	1672	1676	ν (C_4O_{12})
1620			1617	1653	1645	1648	ν (C_2C_3) + ϕ 8a
1599			1597			1642	ν (C_4O_{12}) + Δ ($C_2O_1C_{8a}$)
	1586		1588	1638	1628	1631	ϕ 8a
1580			1579	1600	1595	1628	ϕ 8b
1567						1601	δ $(OH)_{bonded}$
1482	1474		1488	1491	1471	1472	ϕ 19a
1468		1465	1469	1483	1465	1465	ϕ 19b
1432			1439	1418	1420	1420	ϕ 8a + ν (C_2O_1) + δ (OH) + ν (C_2C_9)
	1413	1402			1397	1405	δ (OH) + ϕ 8a + ν (C_2O_1) + ν (C_2C_9)
1388			1399	1361	1335	1397	ϕ 14 + δ (OH)
1341			1347	1347		1358	ϕ 14/ϕ 15 + ν (C_2O_1) + ν (C_3C_4)
1313	1311		1318	1291	1265	1351	ϕ 3 + ν ($C_{8a}O_1C_2$) + δ (C_3H)
1304			1295			1294	ν $(C_9\text{-}O_{10})_{dimer}$ + δ $(O_{10}H)_{dimer}$
1257	1256	1256	1263	1247	1242	1274	ϕ 9a/ϕ 9b + δ (C_3H) + υ (C_4C_{4a}) + ν ($C_{8a}O_1$)
1246						1248	ν ($C_{8a}O_1$) + ν (C_4C_{4a}) + ϕ 9a/ϕ 9b
1235			1234	1231	1217	1220	ϕ 9a/ϕ 9b
1220	1218		1218	1180	1134		ϕ 15 + δ (OH)
1211						1201, 1168	γ $(OH)_{bonded}$
1155	1155		1157	1162	1131	1133	ϕ 15
1134	1140	1127	1143	1131		1131	ϕ 9b + δ (C_3H)
1097	1107		1109		1107	1101	ϕ 9a/ϕ 9b + δ (C_3H)
			1094	1089	1082	1106	δ (C_5H)
1089 sh		1087		1078	1066	1074	ϕ 18b + ν (C_2C_9) + ν (C_2O_1) + δ (C_3H)
1023	1033		1032	1033	1023	1023	ϕ 1
996	1004		1001	989	988	989	ϕ 5
963	972		971	964	958	959	ϕ 16a
944	946		950	941	943	957	Δ ($O_1C_2C_3$)
880	889	894	884	902	894	894	γ (C_3H)
	872	869	865	875	869	869	ϕ 10a
858		854		855	854	865	ϕ 12 + υ ($C_{8a}O_1$)
	786	787	792	784	787	795	ϕ 10b
776			780	769	775	789	ϕ 11 + Γ ($C_2C_9O_{10}$)
	759	766	759	758	761	759	ϕ 11
751				742	742	757	ϕ 6a + Δ ($C_3C_4O_{12}$)
715	718	724	715	680	672	722	Δ ($O_{11}C_9O_{10}$) + ϕ 6a
676	680	680	681	673	677	676	ϕ 4 + Γ ($C_{4a}C_4C_3$)
624	624	615	625	641	644		γ (OH)
596	597	593	601	601	598	607	Δ ($C_3C_4O_{12}$) + ϕ 6b
590				591	587	650	ϕ 6b + Δ ($O_{11}C_9O_{10}$)
537	546	545	540	535	540	553	ϕ 16b + γ (OH)
523	519	515	523	512	511	551	Δ ($C_{4a}C_4C_3$) + Δ ($C_{8a}O_1C_2$)
514				508	508	523	Δ ($C_2C_9O_{10}$) + ϕ 6a
497	500	505	503	483	486	508	Γ ($O_1C_2C_3$) + γ (OH) + ϕ 16a
	430	431	432	427	425	427	ϕ 16a + γ (OH)
412	416		418	420	395	386	Δ ($C_3C_4O_{12}$) + Δ ($C_2C_9O_{10}$)
	347	342	347	345	322	331	Skeletal modes
	310	309	309	306	286	288	Δ ($C_4C_{4a}C_5$)
		296					External mode
	278	275	275	281	265	266	Skeletal modes
		211					DMF[d]
	196		196			213	ν ($OH\cdots O$)[e]
	182		185	182	147		Δ ($C_3C_2C_9$)
	174		174	168	138	133	Skeletal modes
	140		132				External mode
	102			93	93	89	Skeletal modes
	89						External mode
	69			62	61	52	Γ ($O_{11}C_9O_{10}$)
	62						External mode

[a] Atoms are numbered according to Fig. 1. The Wilson notation was used for the description of benzene derivatives normal vibrations (ϕ) [41,42]; for in-plane vibrations: C–C stretching vibrations (8a, 8b, 14, 19a, 19b), C–H/X bending vibrations (3, 18a, 18b), radial skeletal vibrations (1, 6a, 6b, 12) C–H stretching vibrations (2, 20a, 20b, 7a, 7b); for out-of-plane vibrations: C–H/X vibrations (5, 10a, 11, 17a, 17b), skeletal vibrations (4, 16a, 16b). sh – shoulder; vb – very broad band. δ – in-plane deformation, ν – stretching mode, γ – out-of-plane deformation, Δ – in-plane skeletal deformation, Γ – out-of-plane skeletal deformation.
[b] At the B3LYP/6-31G** level, wavenumbers are scaled according to Merrick et al. [20].
[c] For 2CA-1 monomer (Fig. 1), at the LDA/PWSCF level.
[d] Band related to the solvent interaction with 2CA.
[e] Mode relative to ($2CA_c$) dimer.

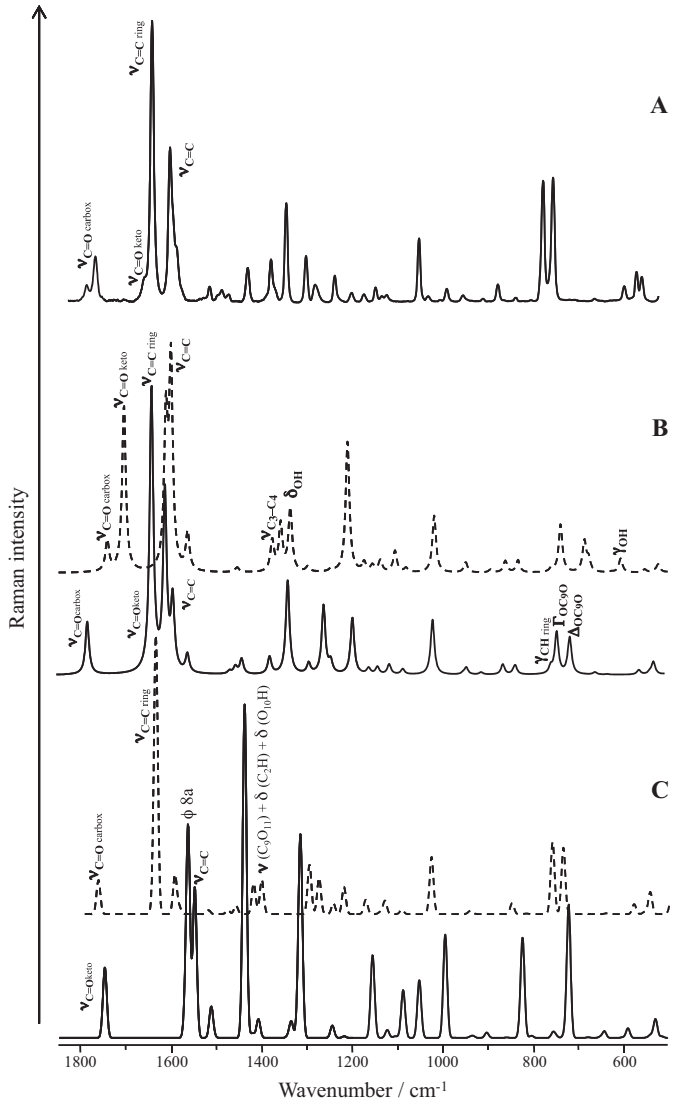

Fig. 4. Raman spectra (500–1800 cm^{-1}) for 3CA. (A) Experimental spectrum for the solid. (B) Calculated spectra (isolated molecule, B3LYP/6-31G**) for the two major 3CA conformers (A): 3CA-1 (solid line) and 3CA-2 (dotted line). (C) Calculated spectra (solid, LDA/PWSCF) for the monomer (dotted line) and the centrosymmetric dimer (solid line) (the atoms are numbered according to Fig. 1).

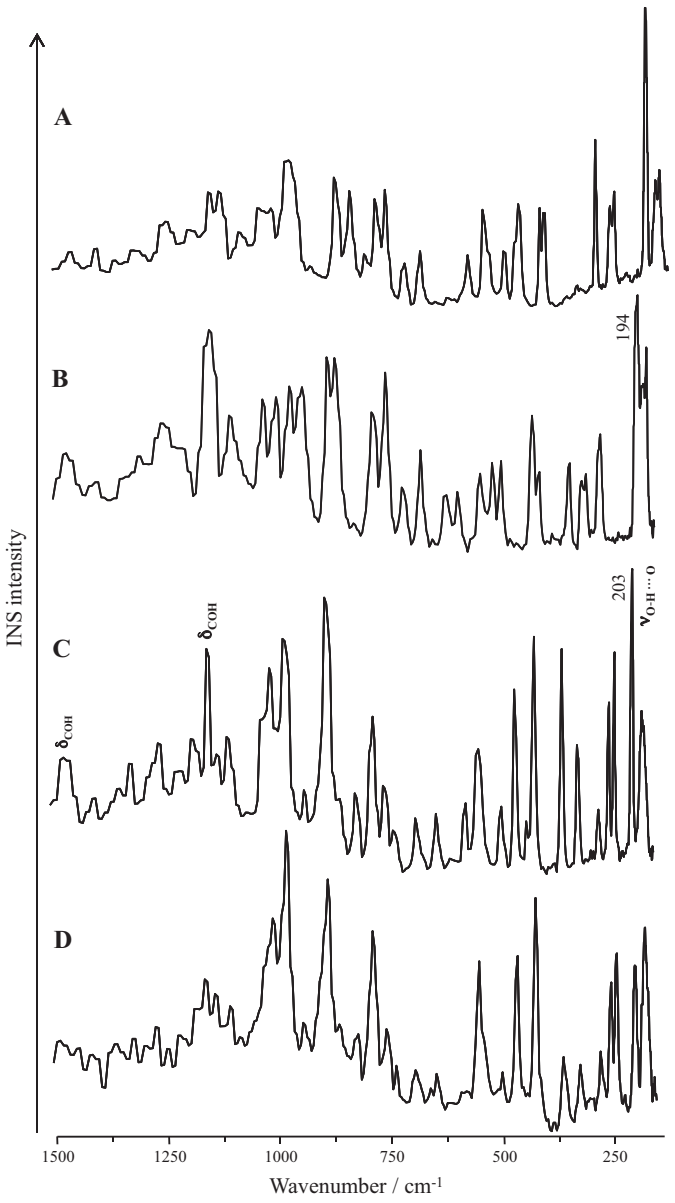

Fig. 5. Experimental INS spectra (150–1500 cm^{-1}) for chromone (A), 2CA (B), 3CA (C) and O-deuterated 3CA (D).

theoretically, Table 2), was substituted by δ_{OD}, at 983 cm^{-1}, due to the combined effect of the H-bond weakening and the oscillator's mass increase.

As to the effect of solvation, it was shown that the intramolecular 6-membered rings formed through these (O—H···O) interactions were disrupted in DMF solution, giving rise to intermolecular H-bonds with the solvent. This was clearly observed for 3CA, for which the $\nu_{OH\cdots O}$ band due to the intramolecular H-bond, at 202 cm^{-1}, was substituted by another at 136 cm^{-1} (Fig. 6), ascribed to the H-interaction with the carbonyl group of the solvent (Table 5). In addition, the chromone's spectral pattern was found to undergo significant changes from the solid to the solution. For the 3-carboxylic derivative, in particular, several bands between *ca.* 1000 and 400 cm^{-1} were absent in the latter as compared to the condensed phase (Fig. 6), suggesting that they may be due to vibrations associated to the 6-membered intramolecular ring formed by the (O—H···O) bridge. These results enable to assume that intramolecular H-bonds are favoured over the intermolecular ones, in the solid. This is particularly true for 3CA, and agrees with the extremely high pK_a value reported for the carboxylic group in this compound (8.85).

The solid state experimental vibrational spectra of the chromones under study are expected to be best described by a plane-wave theoretical approach, which closely represents condensed phase conditions. In fact, as discussed previously, the calculations presently carried out at this level yielded two main dimeric structures for the carboxylic chromone derivatives 2CA and 3CA, either centrosymmetric or non-centrosymmetric, the former being favoured due to strong (O)H···O(=C) intermolecular top-to-top interactions (Fig. 2 and Table 1). Comparison of the PW calculated vibrational profiles, for both the monomeric species and the centrosymmetric dimers, with the corresponding experimental spectra (Raman, FTIR and INS) evidenced a quite good agreement (Tables 2–4, Figs. 3, 4 and 6). For 3CA, in particular, there is a better accordance between the experimental data and the one predicted for the monomer (*e.g.* $\nu_{C4=O}$ calculated at *ca.* 1673 cm^{-1} *vs.* the 1631 cm^{-1} experimental), as expected in view of the high stability of this form as compared to the dimer, due to the favoured

Table 5
Experimental and calculated INS wavenumbers (cm^{-1}) for 3CA, in the solid and in DMF-d_7 solution.

Approximate description	Experimental		Calculated		
	Solid	DMF-d_7	B3LYP[a]	PW[b]	PW (3CAc)[c]
ν (OH···O)	203		202[d]	195	225
ν (OH···O)DMF		136			

[a] At the B3LYP/6-31G** level.
[b] At the LDA/PWSCF level.
[c] At the LDA/PWSCF level, for dimer 3Cac (Fig. 2).
[d] Scaled by a factor of 1.05 [20].

intramolecular (O_{10}—H···O_{12}) bond (Fig. 4). For 2CA, in turn, the dimeric structure (Fig. 2) seems to be preferred over the monomer, which is reflected in the experimental *vs.* theoretical vibrational profiles, a better representation being achieved for the calculated centrosymmetric dimer (Fig. 3).

Additionally, the Raman profile predicted for the dimeric forms of both 2CA and 3CA (Figs. 3 and 4) comprises a strong red shift

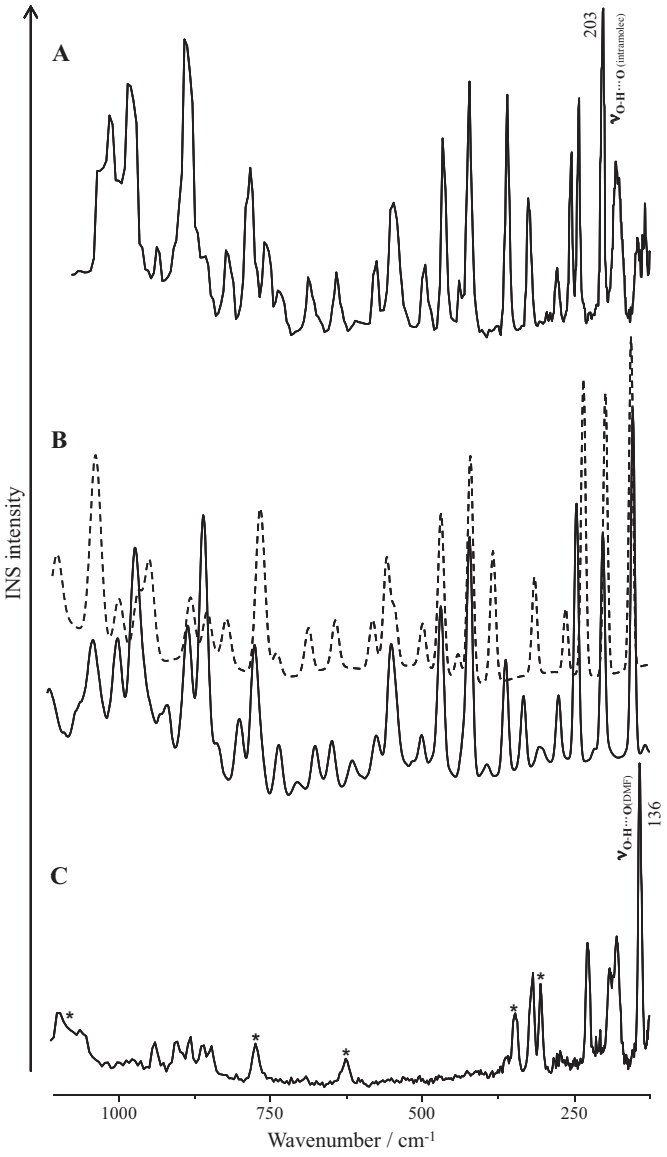

Fig. 6. INS spectra (125–1125 cm^{-1}) for 3CA. (A) Experimental spectrum for the solid. (B) Calculated spectrum for the 3CA-1 conformer: B3LYP/6-31G**, solid line; LDA/PWSCF, dotted line. (C) Experimental spectrum for the solution in DMF-d_7 (the bands of the solvent are marked with an asterisk).

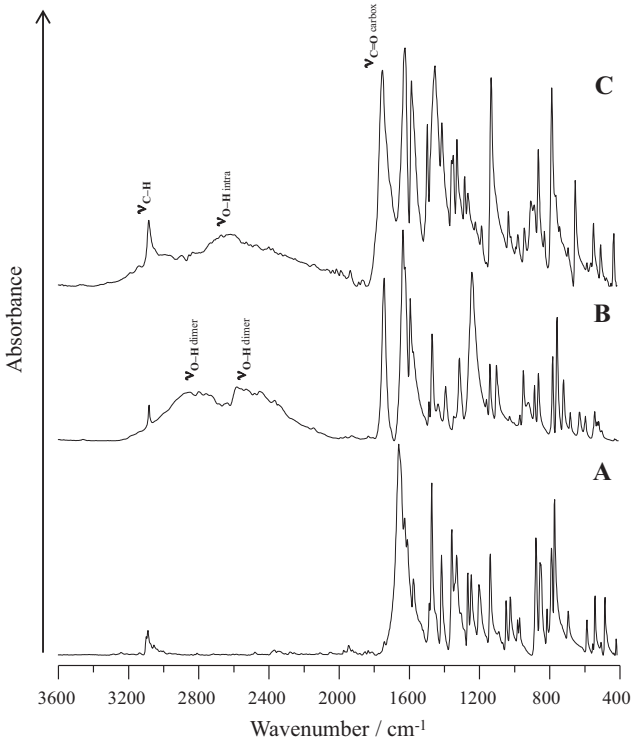

Fig. 7. Experimental FTIR spectra for chromone (A), 2CA (B) and 3CA (C).

of the carboxylic C=O stretching ($\nu_{C9=O11}$) (*e.g.* 1753 cm^{-1} in the monomer *vs.* 1688 cm^{-1} in the dimer, for 2CA, Table 4). This is to be expected, due to the strong top-to-top (O_{10}—H···O_{11}) intermolecular close contacts leading to dimer formation (Fig. 2), which cause a marked decrease of the C_9=O_{11} force constant. For the 3CA derivative, an opposite effect is observed for the carbonyl stretching mode ($\nu_{C4=O12}$) that displays a deviation to high wavenumber (from 1596 cm^{-1} in the monomer to 1750 cm^{-1} in the dimer, Fig. 4), since in this particular case the dimer formation involves the disruption of the intramolecular (O_{10}—H···O_{12}) close contact, thus increasing the C_4=O_{12} bond strength (and the corresponding stretching frequency). This does not occur for the 2-carboxylic chromone, for which $\nu_{C4=O12}$ is considerably less affected by dimerisation (from 1672 cm^{-1} in the monomer to 1676 cm^{-1} in the dimer, Table 4 and Fig. 3), since in the most stable monomeric conformation (Fig. 1) the carbonyl group is not involved in an intramolecular H-bond. Also, these vibrational results appear to reflect a preference for the centrosymmetric dimeric geometry of 2CA over the non-centrosymmetric one (involving the carbonyl group, Fig. 2), that would lead to a substantial variation of the C_4=O_{12} stretching frequency as compared to the monomer.

These hydrogen close contacts, which play an essential role in the conformational equilibrium of the chromone derivatives under study, were reflected in the FTIR spectra (Fig. 7) and also

unequivocally identified by inelastic neutron scattering spectroscopy. In fact, for the 2CA dimer the stretching due to the intermolecular H-bonds ($\nu_{O\cdots H}$), theoretically predicted at about 200 cm^{-1}, was detected experimentally by INS at 196 cm^{-1} (Fig. 5). For 3CA, in turn, the $(O_{10})H\cdots O_{12}(=C)$ intramolecular interaction (with a calculated d = 152 pm in the solid), proposed to be favoured relative to the intermolecular one, gives rise to the INS band at 202 cm^{-1} (Fig. 5), in good accordance with the theoretical feature at 195 cm^{-1}. In addition, the ν_{OH} carboxylic feature was calculated to be strongly shifted from 3600 cm^{-1} to *ca.* 2600–2300 cm^{-1} upon formation of this hydrogen-type interaction (monomer to dimer) (Tables 2 and 4).

4. Conclusions

A conformational analysis of two carboxylic acid chromones – chromone-2-carboxylic acid and chromone-3-carboxylic acid – was carried out, by vibrational spectroscopy and theoretical approaches. The combined analysis of the optical vibrational results (Raman and FTIR) and the complementary INS data gathered for these systems (including their O-deuterated forms) allowed a complete assignment of their vibrational features, as well as a thorough understanding of their H-bonding profile (both intra- and intermolecular) which strongly influences their conformational behaviour. In addition, the high sensitivity of INS in the low wavenumber spectral region allowed the detection of the vibrational modes associated to (O—H···O) interactions taking place within these molecules. Coupling this experimental information to density functional theory and plane-wave calculations, for both the isolated molecule and the solid (monomeric and dimeric structures), led to a thorough understanding of their main conformational preferences, including their H-bonding pattern.

The results presently gathered lead to the assumption that the balance between intra- and intermolecular hydrogen-type interactions is crucial for the conformational behaviour of these systems. For 3CA, intramolecular H-bonds (H···O interactions, yielding a 6-membered ring) are clearly favoured over the intermolecular ones, the opposite being true for 2CA which is suggested to occur as a favoured top-to-top dimer in the condensed phase. This is in accordance with the extremely high pK_a value previously reported for the 3-carboxylic chromone (8.85 [35] and presently calculated as 8.70), in contrast to 2CA's pK_a (2.55 [36], currently calculated as 3.02).

Special attention should be paid to the close relationship between structural conformation and activity of these chromone derivatives, in view of attaining a better understanding of their well recognised antioxidant properties (which are being evaluated in a parallel study). Only a detailed understanding of the conformational behaviour of this group of phytochemicals may allow a rational design of optimised chemotherapeutic and/or chemopreventive chromone-based agents, with improved efficacy and safety.

Acknowledgements

The authors thank financial support from the Portuguese Foundation for Science and Technology – PEst-OE/QUI/UI0070/2011 and PhD fellowship SFRH/BD/40235/2007. The INS work has been supported by the European Commission under the 7th Framework Programme through the Key Action: Strengthening the European Research Area, Research Infrastructures. Contract No.: CP-CSA_INFRA-2008-1.1.1 Number 226507-NMI3.

Appendix A. Supplementary data

Supplementary data associated with this article can be found, in the online version, at http://dx.doi.org/10.1016/j.vibspec.2012.06.010.

References

[1] P. Fresco, F. Borges, C. Diniz, M.P.M. Marques, Med. Res. Rev. 26 (2006) 747–766.
[2] N.F.L. Machado, M.P.M. Marques, Curr. Bioact. Compd. 6 (2010) 76–89.
[3] N.F.L. Machado, C. Ruano, J.L. Castro, M.P.M. Marques, J.C. Otero, Phys. Chem. Chem. Phys. 13 (2011) 1012–1018.
[4] P.C.H. Mithcell, S.F. Parker, A.J. Ramirez-Cuesta, J. Tomkinson, Vibrational spectroscopy with neutrons: with applications in chemistry, biology, materials science and catalysis, World Scientific, Hackensack, NJ, 2001.
[5] http://www.isis.stfc.ac.uk/.
[6] M.J. Frisch, G.W. Trucks, H.B. Schlegel, G.E. Scuseria, M.A. Robb, J.R. Cheeseman, J.A. Montgomery Jr., T. Vreven, K.N. Kudin, J.C. Burant, J.M. Millam, S.S. Iyengar, J. Tomasi, V. Barone, B. Mennucci, M. Cossi, G. Scalmani, N. Rega, G.A. Petersson, H. Nakatsuji, M. Hada, M. Ehara, K. Toyota, R. Fukuda, J. Hasegawa, M. Ishida, V. Nakajima, Y. Honda, O. Kitao, H. Nakai, M. Klene, X. Li, J.E. Knox, H.P. Hratchian, J.B. Cross, C. Adamo, J. Jaramillo, R. Gomperts, R.E. Stratmann, O. Yazyev, A.J. Austin, R. Cammi, C. Pomelli, J.W. Ochterski, P.Y. Ayala, K. Morokuma, G.A. Voth, P. Salvador, J.J. Dannenberg, V.G. Zakrzewski, S. Dapprich, A.D. Daniels, M.C. Strain, O. Farkas, D.K. Malick, A.D. Rabuck, K. Raghavachari, J.B. Foresman, J.V. Ortiz, Q. Cui, A.G. Baboul, S. Clifford, J. Cioslowski, B.B. Stefanov, G. Liu, A. Liashenko, P. Piskorz, I. Komaromi, R.L. Martin, D.J. Fox, T. Keith, M.A. Al-Laham, C.Y. Peng, A. Nanayakkara, M. Challacombe, P.M.W. Gill, B. Johnson, W. Chen, M.W. Wong, C. Gonzalez, J.A. Pople, Gaussian 03 (Revision B.04), Gaussian, Inc., Pittsburgh, PA, 2003.
[7] C. Lee, W. Yang, R.G. Parr, Phys. Rev. B 37 (1988) 785–789.
[8] B. Miehlich, A. Savin, H. Stoll, H. Preuss, Chem. Phys. Lett. 157 (1989) 200–206.
[9] A.J. Becke, Phys. Rev. A 38 (1988) 3098–3100.
[10] A.J. Becke, J. Chem. Phys. 98 (1993) 5648–5652.
[11] G.A. Petersson, A. Bennett, T.G. Tensfeldt, M.A. Al-Laham, W.A. Shirley, J. Mantzaris, J. Chem. Phys. 89 (1988) 2193–2218.
[12] M.J. Frisch, J.A. Pople, J.S. Binkley, J. Chem. Phys. 80 (1984) 3265–3269.
[13] C. Peng, P.Y. Ayala, H.B. Schlegel, M.J. Frisch, J. Comput. Chem. 17 (1996) 49–56.
[14] E. Cancès, B. Mennucci, J. Tomasi, J. Chem. Phys. 107 (1997) 3032–3041.
[15] B. Mennucci, E. Cancès, J. Tomasi, J. Phys. Chem. B 101 (1997) 10506–10517.
[16] E. Cancès, B. Mennucci, J. Math. Chem. 23 (1998) 309–326.
[17] V. Barone, M. Cossi, J. Tomasi, J. Comput. Chem. 19 (1998) 404–417.
[18] R. Cammi, J. Tomasi, J. Comput. Chem. 16 (1995) 1449–1458.
[19] S. Miertus, E. Scrocco, J. Tomasi, J. Chem. Phys. 55 (1981) 117–129.
[20] J.P. Merrick, D. Moran, L. Radom, J. Phys. Chem. A 111 (2007) 11683–11700.
[21] T. Van Voorhis, G.E. Scuseria, J. Chem. Phys. 109 (1998) 400–410.
[22] M.T. Benson, M.L. Moser, D.R. Peterman, A. Dinescu, J. Mol. Struct. THEOCHEM 867 (2008) 71–77.
[23] A.E.L. Reed, A. Curtiss, F. Weinhold, Chem. Rev. 88 (1998) 899–926.
[24] E.D. Glendening, A.E.L. Reed, J.E. Carpenter F. Weinhold, NBO Version 3.1.
[25] J.P. Perdew, A. Zunger, Phys. Rev. B 23 (1981) 5048–5079.
[26] P. Giannozzi, S. Baroni, N. Bonini, M. Calandra, R. Car, C. Cavazzoni, D. Ceresoli, G.L. Chiarotti, M. Cococcioni, I. Dabo, A. Dal Corso, S. De Gironcoli, S. Fabris, G. Fratesi, R. Gebauer, U. Gerstmann, C. Gougoussis, A. Kokalj, M. Lazzeri, L. Martin-Samos, N. Marzari, F. Mauri, R. Mazzarello, S. Paolini, A. Pasquarello, L. Paulatto, C. Sbraccia, S. Scandolo, G. Sclauzero, A.P. Seitsonen, A. Smogunov, P. Umari, R.M. Wentzcovitch, J. Phys.: Condens. Matter 21 (2009) 395502.
[27] U. von Barth, R. Car, personal communication.
[28] N. Troullier, J.L. Martins, Phys. Rev. B 43 (1991) 1993–2006.
[29] H.J. Monkhorst, J.D. Pack, Phys. Rev. B 13 (1976) 5188–5192.
[30] S. Yip, Handbook of Materials Modeling, vol. 1, Springer, New York, 2005.
[31] D. Michalska, R. Wysokinski, Chem. Phys. Lett. 403 (2005) 211–217.
[32] S.I. Gorelsky, SWizard Program, University of Ottawa, Canada, 2010, http://www.sg-chem.net/.
[33] S.I. Gorelsky, A.B.P. Lever, J. Organomet. Chem. 635 (2001) 187–196.
[34] A.J. Ramirez-Cuesta, Comput. Phys. Commun. 157 (2004) 226–238.
[35] H. Tanaka, P.L. Wang, M. Namiki, Agric. Chem. Biol. Tokyo 36 (1972) 2511–2517.
[36] M.K. Church, H.O.J. Collier, G.W.L. James, Br. J. Pharmacol. 46 (1972) 56–65.
[37] L.F. Holroyd, T. Van Mourik, Chem. Phys. Lett. 442 (2007) 42–46.
[38] Y. Zhao, O. Tishchenko, D.G. Truhlar, J. Phys. Chem. B Lett. 109 (2005) 19046–19051.
[39] G.I. Csonka, A.D. French, V. Johnson, C.A. Stortz, J. Chem. Theor. Comput. 5 (2009) 679–692.
[40] L.X. Hong, T.Z. Xin, Z.X. Zhou, J. Mol. Struct. THEOCHEM 900 (2009) 50–54.
[41] E.B. Wilson Jr., Phys. Rev. 45 (1934) 706–714.
[42] G. Varsányi, Assignments for Vibrational Spectra of Seven Hundred Benzene Derivatives, Adam Hilger Ltd., UK, 1974.